Agricultural and Forest Meteorology 263 (2018) 118–129

Contents lists available at ScienceDirect

Agricultural and Forest Meteorology

journal homepage: www.elsevier.com/locate/agrformet

Trends in evapotranspiration and their responses to climate change and vegetation greening over the upper reaches of the Yellow River Basin

Shiqin Xu[a,b], Zhongbo Yu[a,b,*], Chuanguo Yang[a,b], Xibin Ji[c], Ke Zhang[a,b]

[a] State Key Laboratory of Hydrology–Water Resources and Hydraulic Engineering, Hohai University, Nanjing, Jiangsu Province, China
[b] College of Hydrology and Water Resources, Hohai University, Nanjing, Jiangsu Province, China
[c] Linze Inland River Basin Research Station, Key Laboratory of Ecohydrology in Inland River Basin, Northwest Institute of Eco–Environment and Resources, Chinese Academy of Sciences, Lanzhou 730000, China

ARTICLE INFO

Keywords:
Evapotranspiration
Complimentary relationship
Asymmetric climate warming
Vegetation greening
Cold mountain region

ABSTRACT

This study comprehensively analyzed long-term (1960–2014) variations of potential and actual evapotranspiration (ET) and quantified their inter-annual and seasonal sensitivity and attribution to climate and vegetation growth changes in the upper reaches of the Yellow River Basin (UYRB). Satellite-derived vegetation greenness and in situ measured hydrometeorological datasets were used. Average annual reference evapotranspiration (ET_0) showed significant decreasing trend ($p < 0.05$) by 0.32 mm year^{-1} over the past 55 years. Results obtained from recovered stationary series and sensitivity analyses showed that reduction of wind speed was the major driving force for decreasing trends in annual and seasonal ET_0. Water budget-derived actual evapotranspiration (ET_a) increased dramatically during the study period, whereas potential evapotranspiration (ET_p) calculated from Penman equation and pan evaporation (ET_{pan}) decreased significantly, suggesting the existence of evaporation paradox over the UYRB. ET_a and ET_p or ET_{pan} exhibited complementary behavior, while the complementary relationship was asymmetric. During the period 1982–2014, vegetation greening occurred in most areas (65.6%) of the UYRB and was mediated by elevation. Interestingly, non-uniform climate warming imposed opposite impacts on vegetation growth, namely inter-annual and seasonal NDVI was stimulated by daytime temperature but suppressed by nighttime temperature. Furthermore, the positive impacts imposed by daytime temperature on NDVI was much larger in spring than in autumn and summer. Large-scale coherent vegetation greening would be the primary factor affecting inter-annual ET_a in comparison with climate factors. These results help in deep understanding the hydrological response to climate change in cold mountain regions.

1. Introduction

Evapotranspiration, ET, is the process that water transferredfrom the land surface to the atmosphere. It is the sole term occurred in the water balance budget and energy balance budget. Climate warming is expected to intensify hydrological circle and thus to alter ET (Jung et al., 2010). The theoretical basis for this intensification is summarized in the well-known Clausius-Clapyeron relation that implies that specific humidity would increase approximately exponentially with temperature (Huntington, 2006). Long-term variations of annual ET would be an excellent indicator of the intensity of the hydrological cycle due to its central role in hydrological circle. Unfortunately, world-wide monitoring of ET is still limited and the period of record is very short. Identifying ET trends from basin, regional and continental scale water balance has recently become the focus of the studies on hydroclimatic changes.

Different terms are used to describe the ET, and it is very important to distinguish them for detecting the causes of their variation. Introduced by Thornthwaite (1948) and formally defined by Penman (1956), the term “potential evapotranspiration”, ET_p, indicates the maximum quantity of water capable of being evaporated from soil and transpired from vegetation of a specific surface. For encouraging the use of a standard ET_p, the concept of ‘crop reference evapotranspiration’ (ET_0) was developed and the Penman-Monteith approach (Monteith, 1965) was unanimously accepted as the sole method by the Food and Agricultural Organization (FAO). It is defined as “the rate of evapotranspiration from a hypothetical reference crop with an assumed crop height of 0.12 m, a fixed surface resistance of 70 s m^{-1}, and an albedo of 0.23″ (Allen et al., 1998). Pan evaporation (ET_{pan}) means evaporation observed from an evaporation pan. Actual

* Corresponding author at: State Key Laboratory of Hydrology–Water Resources and Hydraulic Engineering, Hohai University, Nanjing, Jiangsu Province, China.
E-mail addresses: xushiqin@hhu.edu.cn (S. Xu), zyu@hhu.edu.cn (Z. Yu), cgyang@hhu.edu.cn (C. Yang), xuanzhij@ns.lzb.ac.cn (X. Ji), kzhang@hhu.edu.cn (K. Zhang).

https://doi.org/10.1016/j.agrformet.2018.08.010
Received 5 March 2018; Received in revised form 17 June 2018; Accepted 17 August 2018
Available online 27 August 2018
0168-1923/ © 2018 Published by Elsevier B.V.

evapotranspiration (ET_a) is driven essentially by climatic factors, mediated by the vegetation and soil characteristics and constrained by the amount of available water, which is considered the most complicated component of the hydrological cycle (Zhang et al., 2016). In previous studies, only one term or two terms was selected for different ET research purposes at basin or regional scale. Comprehensively analyzing the temporal trends and causes of potential and actual ET is still limited for exploring hydrological response to climate change.

Observations of decreasing ET_{pan} or ET_p in different regions throughout the word have been reported by numerous studies over the past 50 years (Hobbins et al., 2004). This declining trend, however, contrasts with the reported general increases in ET_a in the same period (Teuling et al., 2009). The contradiction between ET_a and ET_{pan} or ET_p is called the evaporation paradox. In the literature, three hypotheses have been proposed to explain this contradiction. The complementary relationship proposed by Bouchet (1963) indicates that ET_{pan} and ET_a should diverge from each other when the land dries; thus Brutsaert and Parlange (1998) suggested that a decrease in ET_{pan} could signal an increase in ET_a. Roderick et al. (2009) showed a new proof that globally observed decreasing solar radiation mainly accounts for the decreasing ET_{pan} trend. The Budyko framework was proposed to reconcile the above conflict (Roderick and Farquhar, 2011). It stated that evaporation was limited by available water (indicated by precipitation) in nonhumid region or by available energy (indicated by ET_p) in humid region. Therefore, in nonhumid region, changes in ET_a is negatively correlated with ET_p via precipitation. While in humid region, ET_a changes is controlled by ET_p and decreasing ET_p trends suggested decreasing ET_a (Wang et al., 2016). These conflicting interpretations and other recent studies indicate that further researches are needed for deep understanding the relationship between ET_a and ET_p.

The Yellow River Basin, directly supporting a population of 107 million people, is one of the most important basins in China (McVicar et al., 2007). However, serious water-related issues, such as water shortages, soil erosion and drying up, result in severe ecological and environmental problems, hindering the sustainable development of the region. The upper reaches of the Yellow River Basin (UYRB) contributes approximately 35% of the total annual discharge in disproportion to its 15% area of the entire Yellow River Basin (Hu et al., 2011). Detecting the UYRB long-term ET trends and exploring their responses to climate change is crucial not only for informed hydroclimatic changes in cold mountain regions, but also for evaluating and predicting water resources in the whole Yellow River Basin. Some previous studies focused on detecting temporal trends of potential ET and their causes (Li et al., 2014; Wang et al., 2012). While a more reliable result, obtained by using a longer observational dataset and comprehensive analyses of the trends in potential and actual ET terms, is required to clarify the possible impacts of climate change on hydrological processes in this region. Moreover, as vegetation greening and climate change both promoted rises of global or regional ET_a (Jin et al., 2017), identifying the main drivers for ET_a changes is critical for accurate prediction of long-term water and energy fluxes; this is especially important in the UYRB, because the prediction accuracy of ET_a from hydrological model and remote sensing retrieval algorithm significantly decreased due to its special Tibetan Plateau environment and complex topography (Li et al., 2014; Xue et al., 2013).

Over the past five decades, temperature data show faster warming in nighttime than in daytime, and in winter than in other seasons (Hartmann et al., 2013). As daytime and nighttime temperature affects vegetation photosynthetic activity in different ways, this non-uniform climate warming may underpin regional differences in the response of ecosystem productivity to warming. It will pose a great challenge to the prediction of future feedbacks between climate and energy/carbon cycle. Implications of such diurnal and seasonal asymmetric warming on vegetation productivity are also investigated in present study for better understanding the responses of montane ecosystem processes to climate warming.

Based on long-term hydrometeorological observations and NDVI data from the Advanced Very High Resolution Radiometer (AVHRR) over the UYRB, we aim (1) to detect the temporal trends of evapotranspiration and pan evaporation at both annual and seasonal scales, (2) to investigate how the trends of reference evapotranspiration are affected by net radiation, air temperature, and wind speed, (3) to validate the evaporation paradox and to clarify whether the actual and potential evapotranspiration rates follow the Bouchet's symmetric complementary relationship, and (4) to examine the impact of asymmetric climate warming on vegetation growth and to evaluate the role of climate change and vegetation greening on ET_a changes.

2. Study area and datasets

2.1. Study area

The UYRB covers an area of about 121 973 km^2 with the Tangnaihai hydrological station as the control outlet of the basin. Its climate belongs to the Tibetan Plateau climate system with distinct wet and dry seasons. The study region is strongly influenced by the summer Indian monsoon and East Asian monsoon (Yao et al., 2012). The average annual precipitation over the UYRB ranges from 350 mm in the northwest to 750 mm in the southeast with a mean value about 522 mm. The annual average temperature varies between -4 and 2 °C from northwest to southeast with a mean value about 0.7 °C. The elevation ranges between 2932 and 6127 m. The land cover of this region is dominated by semi-arid shrubland and alpine grassland.

2.2. Datasets

Meteorological and runoff data. Meteorological data from 1960 to 2014 were provided by the National Meteorological Information Centre of China and can be downloaded from the China Meteorological Forcing Data Sharing Service System (http://data.cma.cn/). There are 19 metrological observatories located on the UYRB, comprising the Qinghai Province, and parts of Sichuan and Gansu provinces. Observation stations were deleted from the dataset if more than 5% of the data from the station was missing, and finally meteorological data from 14 metrological observatories were used in this study. Basic information of these stations, including World Meteorological Organization (WMO) number, name, geographic location, mean annual ET_0, and mean annual ET_{pan} was summarized in the Table 1. Data used in this study were daily precipitation (P, mm), minimum (T_{min}), maximum (T_{max}) and mean (T_{mean}) air temperature (°C), wind speed at 2 m height (u_2, m s^{-1}), sunshine hours (SH, hour), and relative humidity (RH, %). Monthly and annual meteorological data were averaged from daily means. ET_{pan} at each metrological station was measured by using a metal pan, 20 cm in diameter and 10 cm high, which was installed 70 cm above the ground (the China D20 pan). Annual runoff data of the Tangnaihai, Maqu, and Jimai hydrological stations from 1960 to 2014 was provided by the Ministry of Water Resources of China. Due to sparse population density in this region, the runoff data can be approximately considered as natural flow data.

NDVI data. The AVHRR GIMMS-g archive, produced by the Global Inventory Modelling and Mapping Studies (GIMMS) group, is considered the best dataset available for long-term NDVI trend analysis (Beck et al., 2011). The latest version of the 15-day AVHRR GIMMS-3 g NDVI archive with a spatial resolution of 0.083° was selected for the current analyses. This dataset has been corrected for calibration, view, geometry, volcanic aerosols, and another effects not related to vegetation changes (Tucker et al., 2005).

Table 1
Basic information for the national meteorological observatory stations used in this study, and the mean annual reference evapotranspiration (ET_0) and pan evaporation (ET_{pan}) of each station.

WMO number	Name	Longitude (°E)	Latitude (°N)	Altitude (m)	ET_0 (mm)	ET_{pan} (mm)	WMO number	Name	Longitude (°N)	Latitude (°N)	Altitude (m)	ET_0 (mm)	ET_{pan} (mm)
52856	Qiapuqia	100.62	36.27	2835.0	684.1	1738.6	56065	Henan	101.60	34.73	8500	728.7	1335.5
52868	Guizhou	101.43	36.03	2237.1	865.6	1957.8	56067	Jiuzhi	101.48	33.43	3628.5	687.5	1206.2
52943	Xinghai	99.98	35.58	3323.2	632.7	1558.3	56079	Ruo'ergai	102.97	33.58	3439.6	818.9	1297.8
56021	Qumalai	95.78	34.13	4175.0	592.7	1421.1	56151	Banma	100.75	32.93	8530.0	557.8	1299.2
56033	Maduo	98.22	34.92	4272.3	623.4	1340.7	56172	Ma'erkang	102.23	31.90	2664.4	723.4	1525.2
56034	Qingshuihe	97.13	33.80	4415.4	619.3	1143.7	56173	Hongyuan	102.55	32.80	3491.6	819.7	1336.4
56046	Dari	99.65	33.75	3967.5	622.7	1207.4	56182	Songpan	103.57	32.65	2850.7	688.8	1262.1

3. Methods

3.1. Estimating net radiation

Daily net radiation (MJ m^{-2} day^{-1}) was calculated from hours of sunshine due to limitation of radiation observation.

$$R_n = (1-\beta)R_s - R_{nl} \quad (1)$$

where R_s is the solar or shortwave radiation (MJ m^{-2} day^{-1}), R_{nl} is the net outgoing long wave (MJ m^{-2} day^{-1}), and β is the albedo of 0.23 for the hypothetical grass reference. R_s and R_{nl} are estimated as

$$R_s = (a_s + b_s\frac{n}{N})R_a \quad (2)$$

$$R_{nl} = \sigma *(\frac{T_{max,K}{}^4 + T_{min,K}{}^4}{2})(0.34-0.14)(1.35\frac{R_s}{R_{s0}}-0.35) \quad (3)$$

where R_a is the extraterrestrial radiation (MJ m^{-2} day^{-1}), $T_{max,K}$ is the absolute maximum temperature (K = °C + 273.16), $T_{min,K}$ is the absolute minimum temperature (K = °C + 273.16). Regression constant, a_s, is the fraction of extraterrestrial radiation reaching the earth on overcast days (n = 0), and $a_s + b_s$ is the fraction of extraterrestrial radiation reaching the earth on clear days (n = N). The values of a_s and b_s are site specific and can be calibrated based on solar radiation and R_a data. Previous studies used the values recommended by FAO56 (a_s = 0.25 and $a_s + b_s$ = 0.75) if there was no actual solar radiation data available. Ye and Guo (2009) calibrated the regression constants by using observed daily solar radiation and actual sunshine hours from nine meteorological stations on the Tibetan Plateau and obtained statistically significant results with an acceptable range of root-mean-square error. Their recommended values of a_s = 0.24 and $a_s + b_s$ = 0.84 were adopted in this study because there is no solar radiation observatory in the UYRB.

3.2. Calculation of ET_0

The Penman-Monteith method (Allen et al., 1998) is used to calculate ET_0 (mm day^{-1}).

$$ET_0 = \frac{0.408\Delta(R_n-G) + \gamma\frac{900}{T_{mean}+273}u_2 VPD}{\Delta + \gamma(1 + 0.34u_2)} \quad (4)$$

where Δ is the slope of the saturation vapor pressure curve at air temperature (kPa $°C^{-1}$), R_n is the net radiation (MJ m^{-2} day^{-1}), G is the soil heat flux (MJ m^{-2} day^{-1}) and usually can be ignored at daily scale, γ is the psychrometric constant (kPa $°C^{-1}$), T_{mean} (°C) is the mean daily air temperature at 2 m height, u_2 (m s^{-1}) is the wind speed at 2 m height, VPD is the vapor pressure deficit calculated from air temperature and relative humidity (kPa).

3.3. Calculation of ET_a

The water balance method was used to estimate ET_a over the UYRB.

$$ET_a = P - R - \Delta S \quad (5)$$

where P is the total precipitation (mm), R is the runoff (mm), ΔS (mm) is the change in terrestrial water storage and was estimated as the sum of snow water equivalent, soil water and plant canopy surface water from datasets of the Global Land Data Assimilation System (GLDAS) (i.e. GLDAS_NOAH10_M_2.0) (Rodell et al., 2004). Its spatial and temporal resolution is 0.25°and 1 month. Due to limited time cover of the product, ΔS data for the period of 2011–2014 was replaced by the mean value averaged from 1960–2010.

3.4. Complementary relationship

Bouchet (1963) first hypothesized that there are complementary

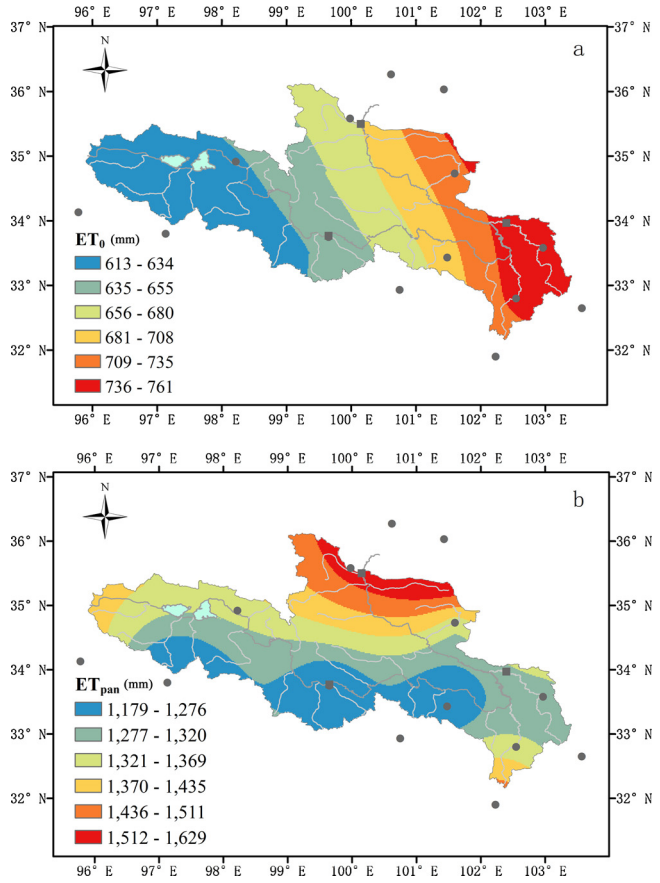

Fig. 1. Spatial distribution of the annual-averaged (a) reference evapotranspiration (ET_0) and (b) pan evaporation (ET_{pan}) during the period of 1960–2014 over the upper Yellow River Basin and the location of meteorological observatories (gray circles) and hydrologic station (gray square).

feedbacks between ET_a and ET_p (Eq. (6)). The key idea behind the complementary relationship (CR) formalism is that as a surface dries, a fraction of the energy not used for evaporation becomes available in the form of increased sensible heat flux that increases potential evaporation and gives rise to a complementary relation between actual and potential evaporation (Brutsaert, 2005). Morton (1969) and Brutsaert and Stricker (1979) further developed the idea and proposed a symmetric CR, which is the widely used Advection Aridity model (Eq. (7)).

$$ET_p - ET_w = b(ET_w - ET_a) \tag{6}$$

$$ET_a = 2ET_w - ET_p \tag{7}$$

where b is a constant of proportionality, ET_w is the wet environment evapotranspiration (mm day^{-1}) and can be estimated by using the Priestley-Taylor equation (Priestley and Taylor, 1972).

$$ET_w = \frac{\alpha\Delta(R_n - G)}{\Delta + \gamma} \tag{8}$$

where α is the well-known Priestley-Taylor coefficient. In the current study, parameter b and α were calibrated by using the genetic algorithms (De-Jong, 1975).

Although ET_0 is a very good representative of ET_p under give conditions, the Penman (1956) equation is used here to estimate ET_p of the CR.

$$ET_p = \frac{0.408\Delta(R_n - G)}{\Delta + \gamma} + \frac{\gamma E_a}{\Delta + \gamma} \tag{9}$$

where E_a is the drying power of the air (mm day^{-1}), calculated by using the Penman's original Rome wind function (Brutsaert, 1982)

$$E_a = 0.26(1 + 0.54u_2)VPD \tag{10}$$

The units of the parameters and variables in Eqs. (8), (9), and (10) are the same as in Eq. (4).

3.5. Contribution estimation and sensitivity analysis

In order to quantify the relative contribution of R_n, T_{mean}, and u_2 to the trends in ET_0 at annual and seasonal scales, a recovered stationary series method was employed as follows (Xu et al., 2006): (1) Trends in R_n, T_{mean}, and u_2 were removed to obtain stationary time series; (2) ET_0 was recalculated from the detrended data series for R_n, T_{mean}, or u_2 while original data for other variables were retained in each time; (3) ET_0 values calculated from the stationary and original time series were compared and the difference was considered as the influence of the trend by that variable.

To fully understand the contribution of each climatic variable to ET_0 changes, a simple but practical way of sensitivity analysis was performed (Wang et al., 2012; Xu et al., 2006). The procedure of this method is: (1) Determining the scenarios of climatic variables by adjusting the observed data series by adding relative changes, setting as 0%, ± 5%, ± 10%, ± 15%, and ± 20% in this study; (2) recalculating the ET_0 by using one scenario at each time; (3) Calculating the relative changes between the recalculated and the original ET_0 against the relative changes in each climatic variable.

3.6. Statistical analysis

To examine spatial distribution of annual-averaged ET_0 and ET_{pan} over the UYRB, the Kriging method with linear variogram was selected as its good performance in mapping ET to extend the observed values to the whole basin (Xu et al., 2006). Linear correlation is used to express the strength of the relation between ET and its drivers. The partial correlation analyses were performed to examine the apparent responses of NDVI to T_{max} and T_{min} to remove the covariate effects between T_{max} and T_{min}. The rank-based Mann-Kendall (MK) statistical test was used to test whether the trends are statistically significant at the 5% significance level or not (Mann, 1945; Kendall, 1975). The trends in ET terms, climatic variables, and NDVI were computed using linear least squares regression. Four seasons are defined in the standard climatological way: spring is defined as occurring from March to May, summer from June to August, autumn from September to November, and winter from December to February.

4. Results

4.1. Spatial patterns and temporal trends of ET_0 and ET_{pan}

Annual-averaged ET_0 and ET_{pan} at each station during the period of 1960–2014 were presented in Table 1. The ET_0 ranged from 557.8 mm $year^{-1}$ to 865.6 mm $year^{-1}$ with a mean value 690.4 mm $year^{-1}$ over the UYRB. The ET_{pan} ranged from 1143.7 mm $year^{-1}$ to 1957.8 mm $year^{-1}$ with a mean value 1402.1 mm $year^{-1}$. Generally, the mean annual ET_0 decreased along with the rise of altitude from southeast to northwest (Fig. 1a). Spatial patterns of the relevant climatic variables including net radiation, mean air temperature, wind speed, and vapor pressure deficit were also examined (data not shown). Consistent spatial distributions between ET_0 and mean air temperature, vapor pressure deficit, and wind speed were found. With regard to the mean annual ET_{pan}, it increased along with the rise of latitude from south to north except a small area in the corner of the southeast UYRB (Fig. 1b). Inconsistent spatial structures between climatic variables and ET_{pan} suggested a complicated spatial patterns in ET_{pan} which might be caused by the combined effect of microclimate and topography.

During the period 1960–2014, ET_0 decreased significantly at 6 meteorological observatories ($p < 0.05$), but increased at 6

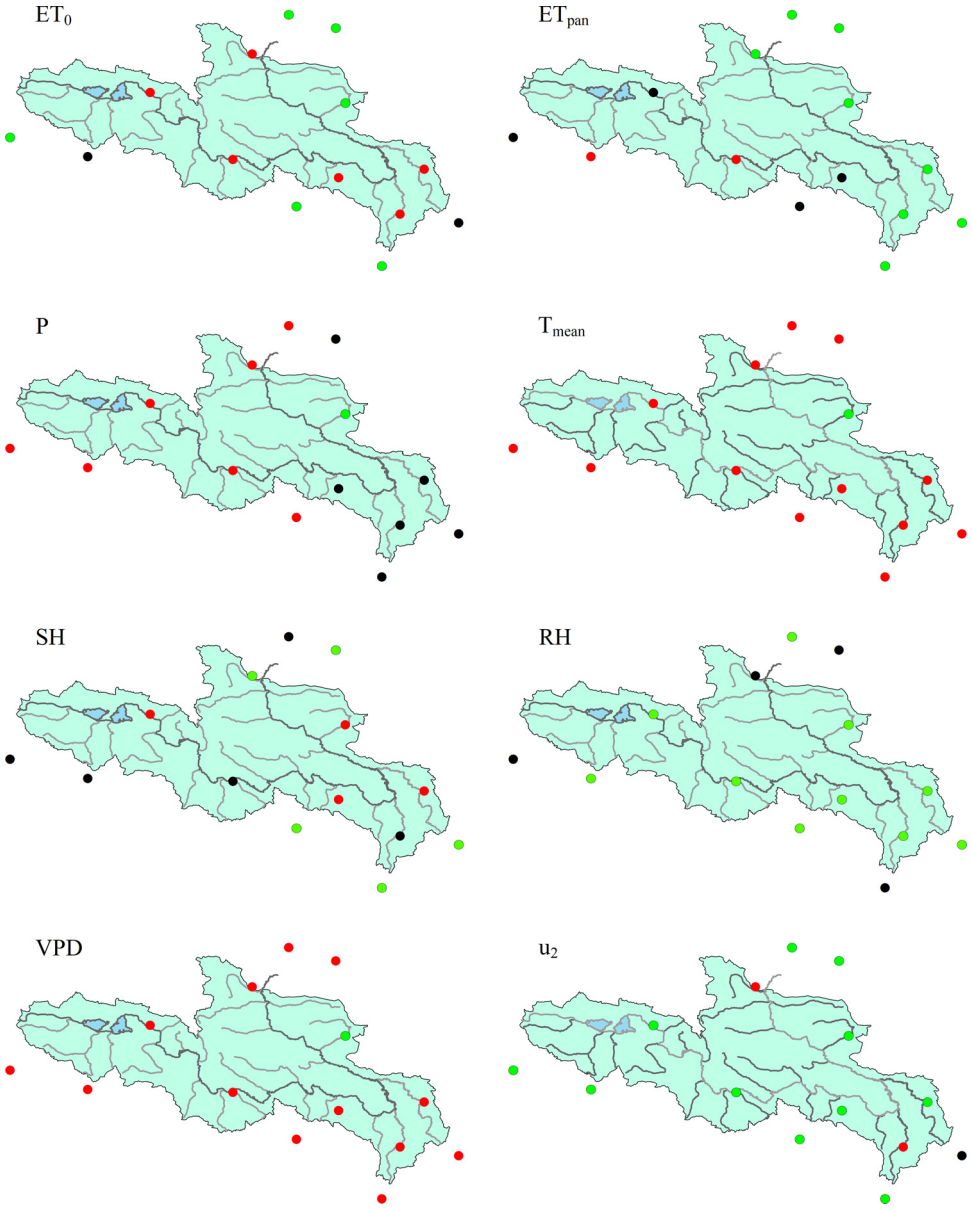

Fig. 2. Temporal variations of annual averaged climate factors during 1960–2014 at each station. The red circle represented a positive significant trend ($p < 0.05$), the green circle represented a negative significant trend ($p < 0.05$), and the black represented a non-significant trend. (For interpretation of the references to colour in this figure legend, the reader is referred to the web version of this article).

meteorological observatories (Fig. 2). ET_{pan} showed a significantly decreasing trend at 8 out of 14 observatories. The trends of climatic variables affecting evapotranspiration were also examined. Precipitation increased significantly at about 50% of the observatories, and most of these sites were located in the west parts of the UYRB. T_{mean} and VPD showed significantly increasing trends at about 93% of observatories, but u_2 showed a decreasing trend at about 79% of observatories and sunshine hour decreased 36% of observatories. Relative humidity decreased at 71% of observatories.

The regionally-averaged interannual ET_0, ET_p, and ET_{pan} over the UYRB showed significantly decreasing trends ($p < 0.05$) from 1960 to 2014, with ET_0 decreasing at 0.32 mm $year^{-1}$, ET_p decreasing at 0.48 mm $year^{-1}$, and ET_{pan} at 4.29 mm $year^{-1}$, respectively (Fig. 3). u_2 also showed a significant decreasing trend, while the decreasing trend of R_n was not significant. T_{mean} showed a significant increasing trend at 0.028 °C $year^{-1}$, which was similar to the increasing rate in the Tibetan Plateau (Zhang et al., 2007). The increasing rate of T_{min} (0.033 °C $year^{-1}$) was 1.3 times that of T_{max} (0.026 °C $year^{-1}$), which suggested an asymmetric warming in daytime and nighttime. For better understanding the climate warming in the UYBR, the annual temperature range, that is, the difference between daytime temperature and nighttime temperature, was plotted in Fig. 4b. A significant reduction in the annual temperature range was found, indicating the difference between T_{max} and T_{min} was decreasing.

Seasonally, ET_0 showed significant decreasing trend in spring and summer but showed a significant increasing trend in winter (Table 2), indicating an uneven distribution of the seasonal variation of ET_0. ET_{pan} showed a significant decreasing trend in spring, summer, and autumn, while showed a no significant increasing trend in winter. For climatic variables, u_2 significantly decreased in four seasons. T_{mean} and VPD, however, significantly increased in four seasons. T_{max}, T_{min} and T_{mean} all increased faster in winter than in other seasons, which suggested that climate warming over the UYRB was not evenly distributed seasonally. The R_n changes in four seasons were not significant.

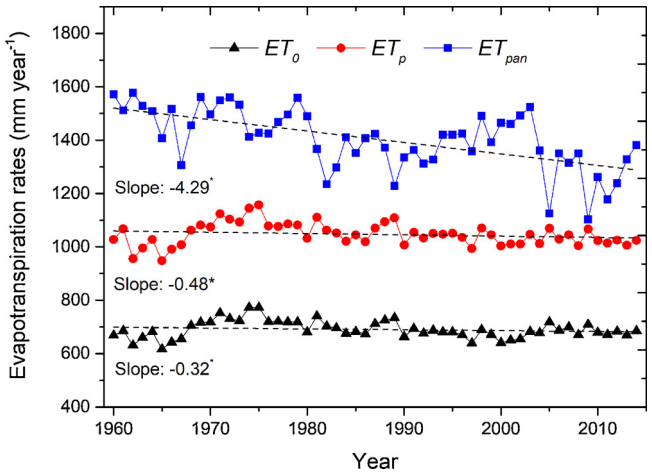

Fig. 3. Temporal variations of yearly reference evapotranspiration (ET_0), potential evapotranspiration (ET_p), and pan evaporation (ET_{pan}) during 1960–2014 over the upper Yellow River Basin. The asterisk represents the trend is significant at $p < 0.05$.

4.2. Contributions of climatic variables to ET_0 trends

In order to quantify the impact of climatic variables on ET_0, three climatic variables including R_n, T_{mean}, and u_2 were detrended and the difference between the original ET_0 and the recalculated ET_0 with detrended climatic series was identified. These contribution analyses were performed at both annual and seasonal scales. The annual original climatic series and the detrended series were plotted in Fig. 4, and the original and recalculated ET_0 series at the annual and seasonal scales were plotted in Fig. 5. From Fig. 4, it can be seen that after detrended, the trend of original climatic series can be extracted and removed, and the original series became stationary time series. Therefore, the difference between the original and the recalculated ET_0 rates could reveal the contribution of climatic variables to the ET_0 trends. At annual scale, when the trend of u_2 was removed, the recalculated ET_0 had a positive trend. However, the trend of the recalculated ET_0 with detrended R_n or T_{mean} series was remain negative, and the differences between the original and recalculated ET_0 rates were very small (Fig. 5a). Therefore, u_2 was recognized as the major driving force for the decreasing trends in annual ET_0. Seasonal ET_0 was also mainly affected by u_2, reflected by great differences between the original and recalculated ET_0 rates with detrended u_2 series in four seasons (Fig. 5b).

In order to fully understand the contribution of climatic variables to

Table 2
Slope of annual and seasonal evapotranspiration and meteorological variables from 1960 to 2014 over the upper Yellow River Basin.[a].

	Annual	Spring	Summer	Autumn	Winter
ET_0	−0.64*	−0.08*	−0.10*	−0.05	0.11*
ET_p	−0.48*	−0.27*	−0.04	−0.08	0.05
ET_{pan}	−4.29*	−1.65*	−1.94*	−0.78*	0.08
R_n	−0.36	0.16	−0.22	0.09	−0.04
T_{mean}	0.028*	0.019*	0.028*	0.027*	0.043*
T_{max}	0.026*	0.015*	0.026*	0.031*	0.040*
T_{min}	0.033*	0.023*	0.039*	0.037*	0.041*
u_2	−0.005*	−0.008*	−0.005*	−0.005*	−0.005*
VPD	0.0005*	0.0003*	0.0010*	0.0005*	0.0004*

[a] The asterisk represents the trend is significant at $p < 0.05$.

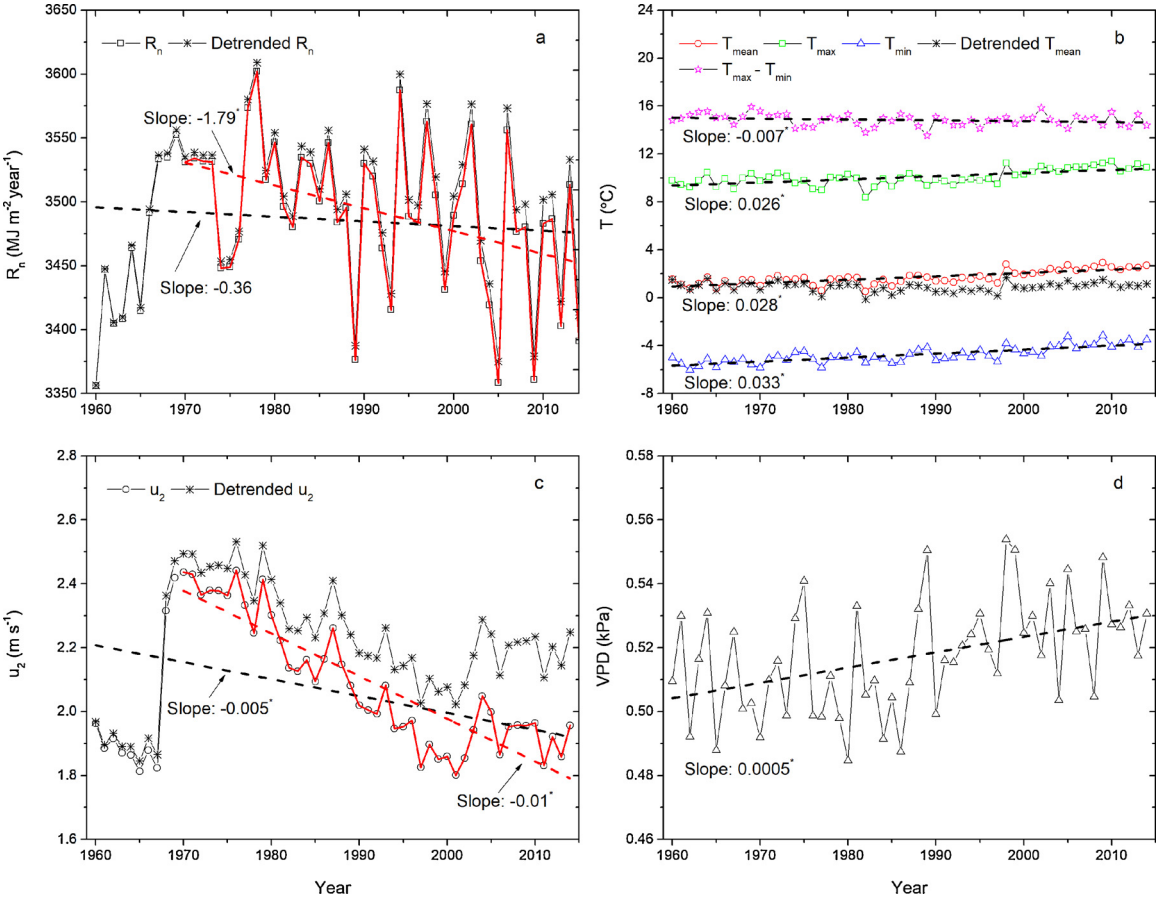

Fig. 4. Temporal variations of yearly (a) net radiation (R_n), (b) minimum (T_{min}), maximum (T_{max}), and mean (T_{mean}) temperature, (c) wind speed at 2 m height, and (d) vapor pressure deficit (VPD) during 1960–2014 over the upper Yellow River Basin. The asterisk represents the trend is significant at $p < 0.05$.

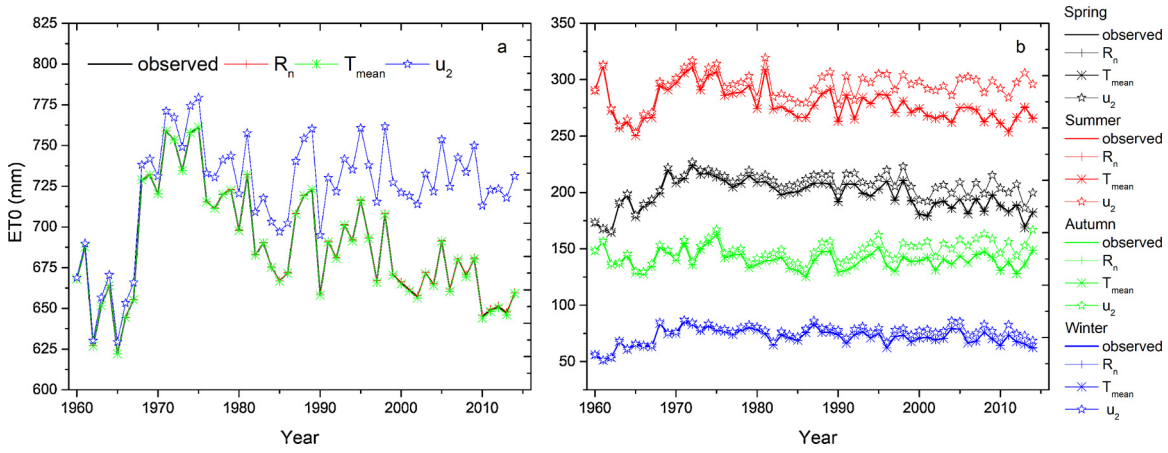

Fig. 5. (a) Inter-annual and (b) seasonal variations in the original reference evapotranspiration (ET_0) and recalculated ET_0 from detrended net radiation (R_n), mean air temperature (T_{mean}), and wind speed at 2 m height (u_2).

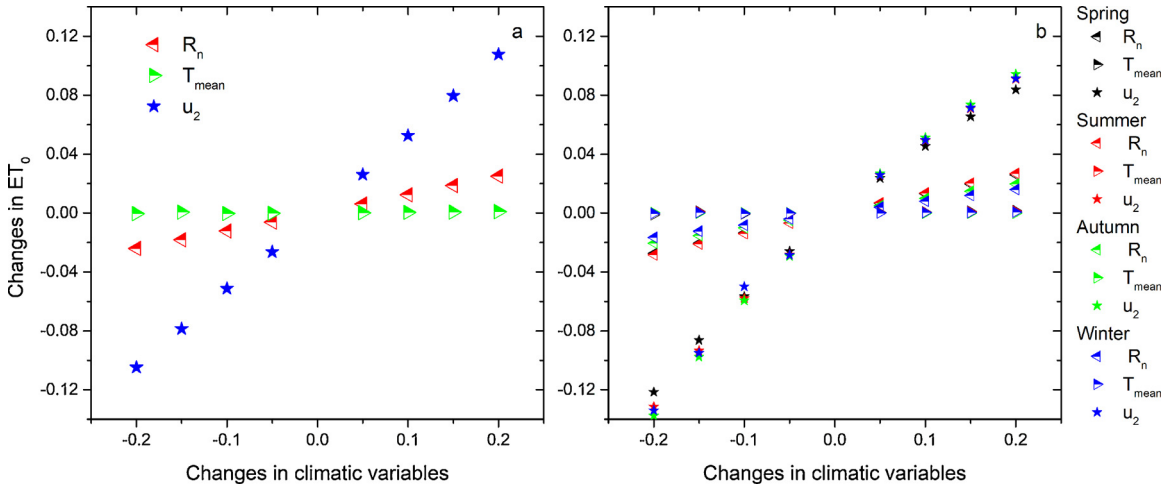

Fig. 6. Sensitivity analyses of (a) annual and (b) seasonal reference evapotranspiration (ET_0) to net radiation (R_n), mean air temperature (T_{mean}), and wind speed at 2 m height (u_2).

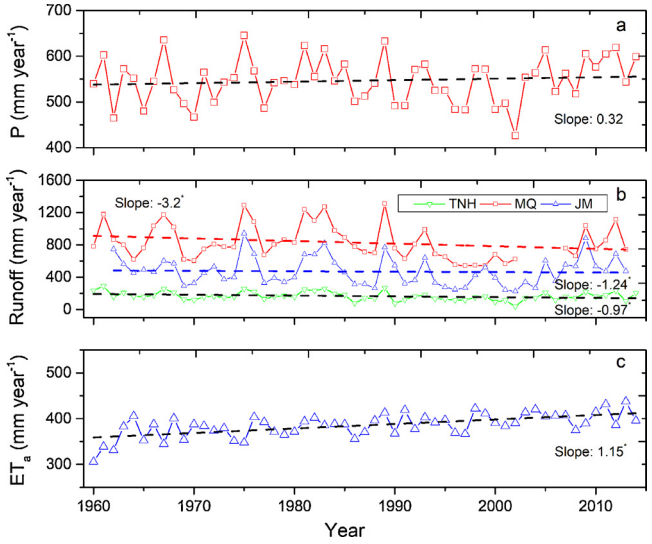

Fig. 7. Temporal variations of yearly (a) precipitation (P_{re}), (b) Runoff from Tangnaihai (TNH), Maqun (MQ), Jimai (JM) hydrological stations and (c) actual evapotranspiration (ET_a) during 1960 to 2014 over the upper Yellow River Basin. The asterisk represents the trend is significant at $p < 0.05$.

ET_0 changes, a widely used sensitivity analysis method was applied with five climate change scenarios. Results of the sensitivity analysis were illustrated in Fig. 6. For the same relative change of the climatic variable, the larger the corresponding relative changes of ET_0, the stronger the sensitivity of the climatic variable. At both annual and seasonal scales, the negative relation of the relative change in ET_0 with u_2 and R_n indicated that ET_0 decreased with decrease of u_2 and R_n. Whereas ET_0 was not sensitive to the change of T_{mean}. It was clear that u_2 was the most sensitive variable for the year and all the seasons, and R_n was the second sensitive variables, while mean temperature exhibited the least sensitivity. Applying the recovered stationary series method and sensitivity analysis, our result showed that the reduction in regional averaged ET_0 was caused by a decrease in u_2 and a decrease in R_n, which was coincident with the causes of the decreasing trend in ET_0 across the Tibetan Plateau (Zhang et al., 2007).

4.3. Testing the Bouchet's complementary relationship

The Bouchet's symmetric complementary relationship (CR) has been widely used to explain the evaporation paradox and to estimate ET_a at different spatiotemporal scales (Kahler and Brutsaert, 2006; Hobbins et al., 2004; Huntington et al., 2011). During the period 1960–2014, inter-annual total precipitation experienced an increasing trend at 0.32 mm year^{-1} even though it failed to pass the significance level test. The inter-annual runoff of Tangnaihai hydrological station significantly

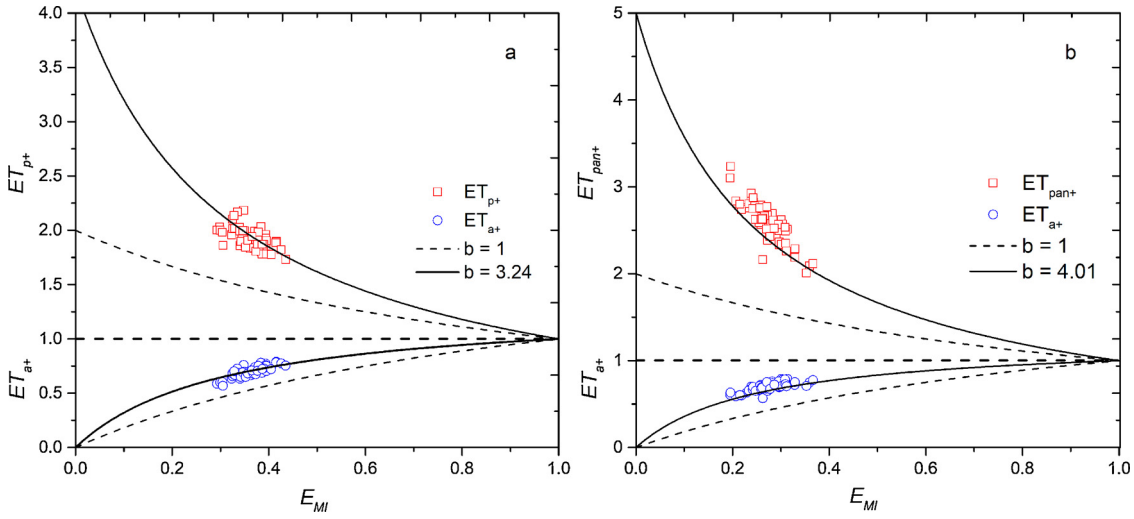

Fig. 8. (a) Plots of the normalized actual evapotranspiration (ET_{a+}) and pan evaporation (ET_{pan+}) against the humidity index, E_{MI} (= ET_a/ET_{pan}). (b) Plots of the normalized actual (ET_{a+}) and the Penman potential (ET_p) evapotranspiration plotted against the E_{MI} (= ET_a/ET_p). The calibrated α equals to 1.20.

decreased at 0.97 mm year^{-1} ($p < 0.05$) (Fig. 7b). Temporal variations of runoff from Maqu and Jimai stations were examined and significant decreasing trends were also observed (Fig. 7b). Water budget-derived ET_a rates significantly increased at 1.15 mm year^{-1} during the study period (Fig. 7c). Considering the decreasing trends in ET_0, ET_p, and ET_{pan} (Fig. 4), it can be reasonably inferred that the evaporation paradox exists in the UYBR.

In order to determine whether the pan evaporation paradox was caused by Bouchet's symmetric CR, the annual observed ET_a values, calculated ET_p values from the Penman equation, and ET_{pan} data were plotted in Fig. 8, against the humidity index. It was clearly evident that a complementary relationship between ET_a and ET_p existed, in which the difference between ET_a and ET_p or ET_{pan} increased with the decrease of humidity index. The ratio of ET_a + ET_p to ET_w (i.e. the parameter b in Eq. (6) was 3.24 and the ratio of ET_a + ET_{pan} to ET_w was 4.01, much larger than 2 in Eq. (7). Such a magnitude of this ratio indicated an asymmetric CR between ET_a and ET_p over the UYRB.

4.4. Vegetation greening and its response to climate warming

Changes in annual NDVI from 1982 to 2014 was illustrated in Fig. 9. The relative contribution of pixels with significant decreasing trends, no significant trends, and significant increasing trends to total pixels was 3.9%, 30.5%, and 65.6%, respectively. Therefore, vegetation greening occurred in most areas in the UYRB (Fig. 9a). When the relationship between NDVI changes and elevation was examined, we found that more than 53% pixels with higher NDVI increasing rates distributed between 4100 m and 4700 m. Above or below this range, the number of pixels or increasing rates significantly decreased (Fig. 9b). Therefore, changes in NDVI was mediated by elevation.

When the relationship between regionally averaged NDVI and temperature was examined, we found that NDVI was positively related to mean temperature. Interestingly, however, asymmetric effect of daytime and nighttime warming on NDVI was found. Annual NDVI was significantly and positively related to daytime temperature (T_{max}) ($p < 0.01$). Contrary to T_{max}, annual NDVI showed a significant negative correlation with nighttime temperature (T_{min}), indicating a negative impact of increasing T_{min} on NDVI. Similar pattern was also obtained between seasonal NDVI and T_{max} and T_{min} (Fig. 10). In order to further determine the sensitivity of annual and seasonal NDVI to concurrent T_{max} and T_{min}, we regressed the NDVI against T_{max}, T_{min}, and precipitation. As expected, both annual and seasonal NDVI were more sensitive to T_{max} than to T_{min} (Fig. 10). The daytime and nighttime warming over the UYRB also did not evenly distributed seasonally (Table 2). Therefore, how changes in daytime and nighttime temperature during different seasons affect NDVI was investigated. During spring, NDVI predominantly and positively correlated with T_{max}. During summer, both the positive impact of T_{max} and negative impact of T_{min} on NDVI was weaker than in spring. During autumn, the pattern of the correlations between NDVI and T_{max} and T_{min} roughly resembled the springtime pattern.

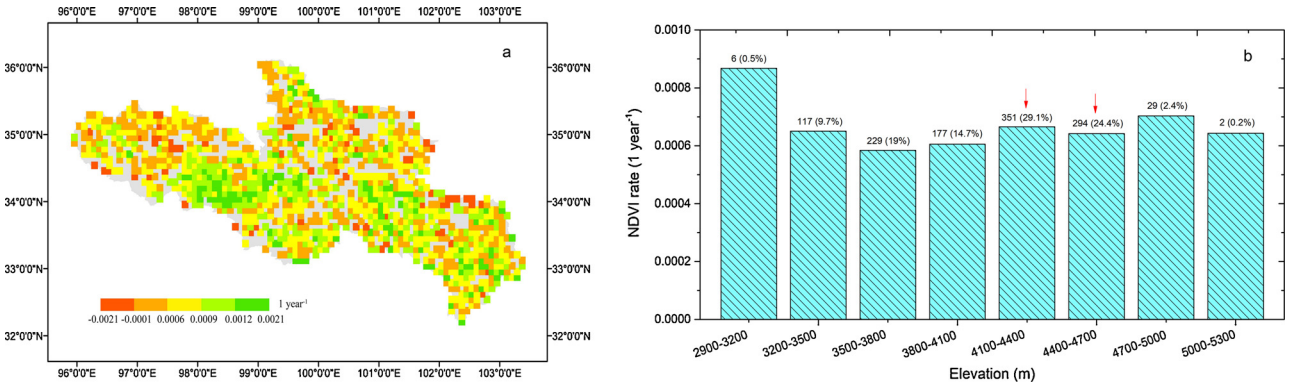

Fig. 9. (a) Changes in annual averaged NDVI from 1982 to 2014 over the upper Yellow River Basin. Only pixels with a statistically significant trend ($p < 0.05$) were colored. (b) Elevation dependency of NDVI changes. The number of pixels within each 300 m elevation interval was given above each bar.

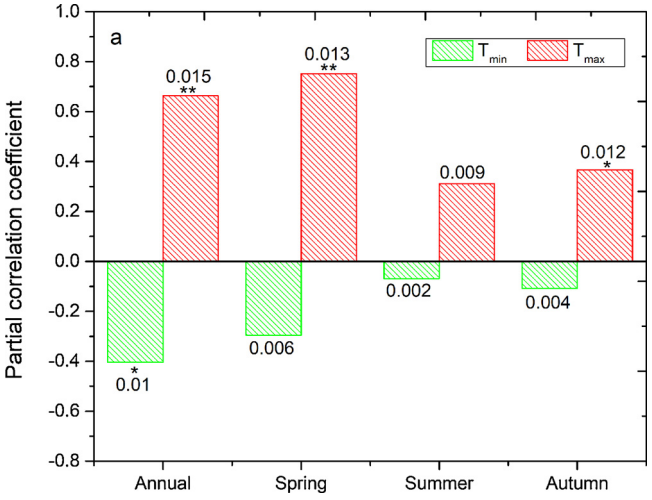

Fig. 10. Partial Correlation coefficient between regionally averaged NDVI and mean air temperature, maximum air temperature, and minimum air temperature. The number above or under the column was the linear regression coefficient between NDVI and T_{max}, T_{min}, and precipitation.

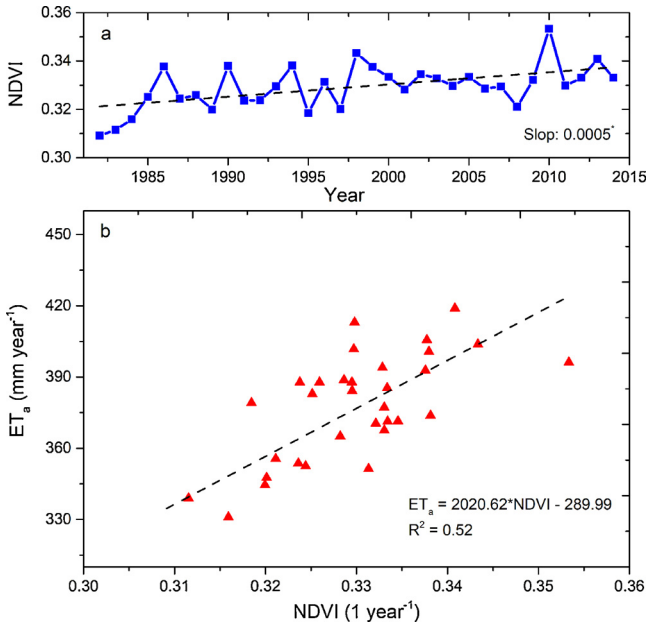

Fig. 11. (a) Temporal variations of annual-averaged NDVI and (b) its relationship with annual actual evapotranspiration (ET_a) rates.

4.5. Responses of ET_a to vegetation greening and climate change

Over 1982–2014, regionally averaged NDVI increased significantly at 0.0005 year^{-1} (Fig. 11a) and showed a positive relationship with concurrent ET_a rates (Fig. 11b). The high correlation coefficient (0.73, significant at 0.01 level) and high determination coefficient ($R^2 = 0.52$) of the linear regression equation between ET_a and NDVI suggested that the trends in inter-annual ET_a were significantly affected by vegetation greening. The bivariate correlations between inter-annual ET_a and precipitation, R_n, T_{mean}, and u_2 were 0.1, −0.05, 0.50 ($p < 0.05$), and −0.35 ($p < 0.05$), respectively. Therefore, air temperature and wind speed were main climatic factors affecting ET_a trends. Then, the partial correlation was used to examine the impacts of climate change (T_{mean} and u_2) and vegetation greening on ET_a trends. The results showed that the correlations between ET_a and NDVI, T_{mean}, and u_2 were 0.62 (significant at 0.01 level), 0.15, and −0.08, respectively. Therefore, vegetation greening would be the primary controller of increasing ET_a rates in comparison with climate change in the UYRB.

5. Discussion

5.1. Asymmetric CR

Using Penman equation to calculate potential evapotranspiration, our asymmetric CR contradicted previous research which reported a symmetric CR for alpine steppe (Ma et al., 2015) and Nevada shrublands (Huntington et al., 2011). It was mainly because the study area was dominated by heterogeneous semi-arid shrubland and alpine grassland, which was affected by strong advection and secondary circulation (Xu et al., 2017, 2018). Moreover, Ma et al. (2015) calculated the drying power of the air in Eq. (9) using the Moin-Obukhov Similarity (MOS) theory rather than the Rome wind function (Monin and Obukhov, 1954). It may be another reason for our contrary results, because the drying power of the air calculated from MOS is probably smaller than its value calculated from Penman Rome wind function (and hence smaller ET_p). We also found that the ratio of $ET_a + ET_{pan}$ to ET_w was larger than the ratio of $ET_a + ET_p$ to ET_w. It was mainly because the additional solar radiation received by the side of the aboveground pans and the strong heat advection from the heterogeneous environment boosted the available energy to the pans (Kahler and Brutsaert, 2006).

5.2. Different impact of daytime and nighttime warming

In the UYRB, vegetation greening showed greater control by T_{max} than by T_{min}. It was supported by some previous studies. For instance, Peng et al. (2013) found that inter-annual change of growing-season NDVI was significantly and positively related to T_{max} but negatively related to T_{min} in most of the boreal zone, cold mountain regions, and wet temperate regions. Xia et al. (2014) reported that T_{max} imposed positive impacts on terrestrial net primary productivity (NPP) but T_{min} suppressed NPP in high latitude area and cold mountain region. Tan (2015) found that both the spring-time NDVI and gross primary productivity (GPP) significantly and positively correlated with spring-time T_{max} but negatively correlated with T_{min} in the Tibetan Plateau. The positive impact of daytime temperature on NDVI is mainly because in cold mountain regions, photosynthetic activity in most plants are subject to temperature limiting. Daytime warming can enhance photosynthetic enzyme activity (Turnbull et al., 2002), increase soil nitrogen mineralization and availability (Melillo et al., 2002), and extend the growing season (Menzel et al., 2006). Therefor vegetation growth is more sensitive to T_{max}. Night-time warming can influence vegetation productivity in two opposite ways: by enhancing autotrophic respiration (Gu et al., 2008), and by indirectly stimulating plant photosynthesis during the following daytime through decreasing frost risk and physiological regulatory mechanisms (Griffin et al., 2002; Turnbull et al., 2002). Obviously, the negative impact of increased autotrophic respiration was more dominant in the UYRB.

Greater stimulation of vegetation greening by T_{max} in spring than in summer and autumn was also found. It was mainly because spring warming advances the onset of leaf unfolding and associated activities and thus results in an earlier start of the growing season and increases carbon uptake in most ecosystems. In summer, however, vegetation productivity was affected by temperature as well as soil water availability in the studied semi-arid region. In some arid and semi-arid regions where soil water availability frequently falls below a critical threshold, summer warming itself could even negatively affect vegetation activity (Niu et al., 2008; Tan, 2015). The weaker impact of T_{max} on NDVI during autumn in comparison with spring could be attributed to either lower soil moisture, less radiation, plant senescence in the autumn season, or surface soil frost in cold regions (Chapman, 2013).

In this study, the asymmetric effects of daytime and nighttime warming on regionally averaged NDVI across the UYRB were

investigated. Yet both changes in vegetation productivity and their climate controls are also spatially heterogeneous. For example, Xia et al. (2014) reported that, in most areas of tundra and boreal forests, NPP was stimulated by daytime warming, but suppressed by nighttime warming. In contrast, grassland and desert primary production increased with nighttime warming, but decreased in other regions. Peng et al. (2013) found that T_{max} positively correlated with NDVI in most wet and cool ecosystems over boreal regions, but negatively correlated with NDVI in dry temperature regions. However, T_{min} negatively correlated with NDVI in boreal regions, but showed a more complex behavior in dry temperature regions. Regional variations in vegetation productivity changes not only reflect current regional climate signals, but could be enhanced or dampened by different temperature sensitivities across climate and vegetation types (Sherry et al., 2008). Further efforts are needed to explore the spatial variations in the impact of daytime and nighttime warming for better understanding the response of vegetation activity to climate warming in the UYRB.

Large-scale coherent vegetation greening could have important consequences. Over the past 55 years, inter-annual ET_0 significantly decreased in the UYRB. Reduction in wind speed was the primary driving force for decreasing ET_0, and it was also highly related to decreasing Penman-calculated ET_p and ET_{pan}. McVicar et al. (2012) reviewed 148 studies reporting trends in observed terrestrial near-surface wind speeds and synthesized possible causes including atmospheric circulation changes, land surface roughness changes, instrumental or observational drifts, increasing trends in available water, and others. Among these causes, increasing land surface roughness was the most possible cause of decreasing u_2, because vegetation greening occurred in most areas of the UYRB, which could increase land surface roughness thus result in stilling (Vautard et al., 2010). In addition, expanded vegetation productivity may affect individual fitness and population dynamics (Miller-Rushing et al., 2010), promote range expansion and drive changes in community composition (Morin et al., 2008). At the ecosystem level, the significant greening is strengthening the influence of vegetation on ecosystem structure and processes, and on surface energy partition and carbon cycle (Chapman, 2013); these influences could further strengthen the regional atmospheric circumfluence. Besides the widespread vegetation greening, agricultural activities also have strong effect on ET_a changes by altering land cover/use. For example, de Vrese et al. (2016) confirmed that irrigation has a direct effect on regional hydrological cycle. Xing et al. (2018) reported that estimating accuracy of ET_a rates in 96 catchments of China was significantly improved by considering the agricultural activities in the Choudhury's equation (Choudhury, 1999). Characterized by extending cultivation and ecological restoration in the UYRB, further studies need to be carried out to investigate the role of vegetation and agricultural activities in energy exchange and water and mass transfer between the land surface and the atmosphere for better understanding the hydrological response to climate change.

5.3. Research uncertainties

Analyzing temporal trends of climate factors, we found that there was a big jump for yearly R_n and u_2 in about 1970. When the data before 1970 was not considered, the decreasing trends of net radiation and wind speed were more significant (Fig. 4a and c). Examining the temporal trends of different radiation terms, the solar radiation over the UYRB showed a significant decreasing rate at 2.49 MJ m^{-2} $year^{-1}$, while the net outgoing long-wave radiation showed a non-significant decreasing rate at 0.36 MJ m^{-2} $year^{-1}$. The lower decreasing rate should be attributed to the rising temperature. In previous studies, sharp increases in net radiation and wind speed during the period of 1970s were also observed in the Tibetan Plateau (Zhang et al., 2007; Xie and Zhu, 2012; Wang et al., 2013) as well as in the Yellow River Basin (Wang et al., 2012). To date, however, it is still unknown whether this jump was caused by instrumentation or general atmospheric circulation, which could cause uncertainties on the role of net radiation and wind speed in ET_0 changes.

AVHRR data with their long-term global coverage at frequent intervals make it possible to detect vegetation dynamics related to climate change. However, a number of aspects potentially introduce noise in the NDVI dataset due to the AVHRR sensor design and data processing (e.g. satellite orbital drift (Price, 1991), lacking reliable onboard calibration devices (Staylor, 1990), and having a limited set of relatively broad spectral bands compared with modern-day sensors). These effects potentially cause unreliable trends. Several studies have compared AVHRR-NDVI data to NDVI as derived from sensors with better calibration, including Landsat, SPOT-Vegetation (SPOT-VGT), and Moderate Resolution Imaging Spectroradiometer (MODIS). For instance, Brown et al. (2006) compared the time series of the GIMMS-g NDVI data to SPOT-VGT, SeaWiFS, MODIS, and LandSAT ETM + Sensors and reported that the long-term AVHRR-NDVI data can provide reliable record for analyzing vegetation activities. Fensholt et al. (2009, 2012) assessed the quality of GIMMS-3 g NDVI data globally by comparison with the MODIS dataset and concluded that the GIMMS-3 g coarse resolution NDVI data is well-suited for long-term vegetation studies of the arid and semi-arid regions. Despite some general agreement, important differences regards to NDVI trends derived from GIMMS-g NDVI time series have been highlighted from global and regional analyses. For instance, Beck et al. (2011) reported that, in comparison with temporal-change values the GIMMS dataset performed best than other three AVHRR-NDVI datasets. While in both analyses MODIS-NDVI performed better than any AVHRR-NDVI data set. Alcaraz-Segura et al. (2010) compared the temporal trends of burned and unburned sites of boreal forest in central Canada calculated from GIMMS-g NDVI dataset and dataset developed by the Canadian Centre for Remote Sensing (CCRS). The CCRS dataset showed NDVI increased in all burned sites and in 50% of the unburned sites. Surprisingly, the GIMMS dataset did not capture the NDVI recovery in most burned sites and even showed NDVI declines in some burned sites one decade after fire. Although in the case of the latest GIMMS-3 g NDVI data, a particular effort was made to correct for calibration, view, geometry, volcanic aerosols, and another effects not related to vegetation changes (Tucker et al., 2005), these controversial results indicated that one should select NDVI data with caution for climate change research.

6. Conclusion

Using the satellite-derived vegetation greenness and in situ measured hydrometeorological datasets, this study analyzed long-term variations of potential and actual ET and quantified their inter-annual and seasonal sensitivity and attribution to climate and vegetation growth changes over the UYRB. Important findings are summarized as following:

1 During the past 55 years, inter-annual ET_0 significantly decreased at 0.32 mm $year^{-1}$ in the UYRB. Reduction in wind speed was the primary driving force for decreasing ET_0.
2 Water budget-derived ET_a increased markedly during the study period, whereas ET_p calculated from Penman equation and ET_{pan} decreased significantly, suggesting the existence of evaporation paradox over the UYRB. ET_a and Penman-calculated ET_p or ET_{pan} exhibited a complementary behavior, while the complementary relationship was asymmetric.
3 During the period from 1982 to 2014, vegetation greening occurred in most areas of the UYRB and was elevation-dependent. It would be the primary factor affecting ET_a trends in comparison with climate factors.
4 Greater warming in nighttime than in daytime, and in winter than in other three seasons indicated an asymmetric warming in the study area. After removing the correlation between T_{max} and T_{min}, we found that annual NDVI positively related to T_{max}, but negatively

related to T_{min}. Furthermore, the positive impacts imposed by daytime temperature on NDVI was much larger in spring than in autumn and summer.

Our comprehensive analyses of the trends in regionally-averaged potential and actual ET and their causes help in understanding the hydrological response to climate change in cold mountain regions. More attention should be paid to ascertain the cause of the asymmetric effect of climate warming on vegetation productivity which affects surface energy partition and carbon cycle.

Acknowledgements

We thank the editor, the associate editor, and two anonymous reviewers for their helpful and constructive comments for improving the manuscript. This work was funded by the National Key R&D Program of China (Grant No. 2016YFC0402706, 2016YFC0402710); National Natural Science Foundation of China (Grant No. 41271036, 41323001, 51539003, 41471016); National Science Funds for Creative Research Groups of China (No. 51421006); the program of Dual Innovative Research Team in Jiangsu Province and the Special Fund of State Key Laboratory of Hydrology-Water Resources and Hydraulic Engineering (Grant No. 20145027312); the Fundamental Research Funds for the Central Universities (Grant No. 2014B17014).

Appendix A. Supplementary data

Supplementary material related to this article can be found, in the online version, at doi:https://doi.org/10.1016/j.agrformet.2018.08.010.

References

Alcaraz-Segura, D., Chuvieco, E., Epstein, H.E., Kasischke, E.S., Trishchenko, A., 2010. Debating the greening vs. Browning of the North American boreal forest: differences between satellite datasets. Global Change Biol. 16 (2), 760–770. https://doi.org/10.1111/j.1365-2486.2009.01956.x.

Allen, R.G., Pereira, L.S., Raes, D., Smith, M., 1998. Crop evapotranspiration-guidelines for computing crop water requirements. FAO Irrigation and Drainage Paper No. 56, Rome, Italy.

Beck, H.E., McVicar, T.R., van Dijk, A.I.J.M., Schellekens, J., de Jeu, R.A.M., Bruijnzeel, L.A., 2011. Global evaluation of four AVHRR-NDVI data sets: intercomparison and assessment against Landsat imagery. Remote Sens. Environ. 115, 2547–2563. https://doi.org/10.1016/j.rse.2011.05.012.

Bouchet, R.J., 1963. Evapotranspiration réelle et potentielle, signification climatique. Int. Assoc. Sci. Hydrol. 62, 134–142.

Brown, M.E., Pinzon, J.E., Didan, K., Morisette, J.T., Tucker, C.J., 2006. Evaluation of the consistency of long-term NDVI time series derived from AVHRR, SPOT-vegetation, SeaWiFS, MODIS, and Landsat ETM+ sensors. IEEE T. Geosci. Remote 44 (7), 1787–1793. https://doi.org/10.1109/TGRS.2005.860205.

Brutsaert, W., 1982. Evaporation In to the Atmosphere: Theory, History and Applications. 299 pp. Springer, N.Y.

Brutsaert, W., 2005. Hydrology: An Introduction. Cambridge Univ. Press, N. Y.

Brutsaert, W., Parlange, M.B., 1998. Hydrologic cycle explains the evaporation paradox. Nature 396 (30). https://doi.org/10.1038/23845.

Brutsaert, W., Stricker, H., 1979. An advection-aridity approach to estimate actual regional evapotranspiration. Water Resour. Res. 15 (2), 443–450. https://doi.org/10.1029/WR015i002p00443.

Chapman, D.S., 2013. Greater phenological sensitivity to temperature on higher Scottish mountains: new insights from remote sensing. Global Change Biol. 19, 3463–3471. https://doi.org/10.1111/gcb.12254.

Choudhury, B.J., 1999. Evaluation of an empirical equation for annual evaporation using field observations and results from a biophysical model. J. Hydrol. 216, 99–110. https://doi.org/10.1016/S0022-1694(9800293-5.

de Vrese, P., Hagemann, S., Claussen, M., 2016. Asian irrigation, African rain: remote impacts of irrigation. Geophys. Res. Lett. 43, 3737–3745. https://doi.org/10.1002/2016GL068146.

De-Jong, K.A., 1975. An Analysis of the Behavior of a Class of Genetic Adaptive Systems, Ph.D. Thesis. University of Michigan, 1975.

Fensholt, R., Rasmussen, K., Nielsen, T.T., Mbow, C., 2009. Evaluation of earth observation based long term vegetation trends-intercomparing NDVI time series trend analysis consistency of Sahel from AVHRR GIMMS, Terra MODIS and SPOT VGT data. Remote Sens. Environ. 113 (9), 1886–1898. https://doi.org/10.1016/j.rse.2009.04.004.

Fensholt, R., Langanke, T., Rasmussen, K., Reenberg, A., Prince, S.D., Tucker, C., Scholes, R.J., Le, Q.B., Bondear, A., Eastman, R., Epstein, H., Gaughan, A.E., Hellden, U., Mbow, C., Olsson, L., Paruelo, J., Schweitzer, C., Seaquist, J., Wessels, K., 2012. Greenness in semi-arid areas across the globe 1981-2007-an earth observing satellite based analysis of trends and drivers. Remote Sens. Environ. 121 (2), 144–158. https://doi.org/10.1016/j.rse.2012.01.017.

Griffin, K.L., Turnbull, M., Murthy, R., Lin, G., Adams, J., Farnsworth, B., Mahato, T., Bazing, G., Potasnak, M., Berry, J., 2002. Leaf respiration is differentially affected by leaf vs. Stand-level night-time warming. Glob. Change Biol. 8, 479–485. https://doi.org/10.1046/j.1365-2486.2002.00487.x.

Gu, L., Hanson, P.J., Post, W.M., Kaiser, D.P., Yang, B., Nemani, R., Pallardy, S.G., Tilden, M., 2008. The 2007 eastern US spring freezes: increased cold damage in a warming world? Bioscience 58, 253–262. https://doi.org/10.1641/B580311.

Hartmann, D.L., Tank, A.M.G.K., Rusicucci, M., Alexander, L., Broenniman, B., Charabi, Y., Dentener, F.J., Dlugokencky, E.J., Easterling, E.R., Kaplan, A., Brian, S., Thorne, P.W., Wild, M., Zhai, P.M., Kent, E., 2013. Observations: atmosphere and surface. In: Stocker, T.F., Qin, D., Plattner, G.K., Tignor, M., Allen, S.K., Boschung, J., Nauels, A., Xia, Y., Bex, V., Midgley, P.M. (Eds.), Climate Change 2013: The Physical Science Basis. Contribution of Working Group I to the Fifth Assessment Report of the Intergovernmental Panel on Climate Change. Cambridge University Press, Cambridge, pp. 159–254.

Hobbins, M.T., Ramírez, J.A., Brown, T.C., 2004. Trends in pan evaporation and actual evapotranspiration across the conterminous US: paradoxical or complementary? Geophys. Res. Lett. 31https://doi.org/10.1029/2004GL019846. L13503.

Hu, Y., Maskey, S., Uhlenbrook, S., Zhao, H., 2011. Streamflow trends and climate linkages in the source region of the Yellow River. China. Hydrol. Process. 25 (22), 3399–3411. https://doi.org/10.1002/hyp.8069.

Huntington, T.G., 2006. Evidence for intensification of the global water cycle: review and synthesis. J. Hydrol. 319, 83–95. https://doi.org/10.1016/j.jhydrol.2005.07.003.

Huntington, J.L., Szilagyi, J., Tyler, S.W., Pohll, G.M., 2011. Evaluating the complementary relationship for estimating evapotranspiration from arid shrublands. Water Resour. Res. 47 (5), 143–158. https://doi.org/10.1029/2010WR009874.

Jin, Z., Liang, W., Yang, Y., Zhang, W., Yan, J., Chen, X., Li, S., Mo, X., 2017. Separating vegetation greening and climate change controls on evapotranspiration trend over the Loess Plateau. Sci. Rep. 7, 8191. https://doi.org/10.1038/s41598-017-08477-x.

Jung, M., Reichstein, Ciais, M.P., et al., 2010. Recent decline in the global land evapotranspiration trend due to limited moisture supply. Nature 467, 951–954. https://doi.org/10.1038/nature09396.

Kahler, D.M., Brutsaert, W., 2006. Complementary relationship between daily evaporation in the environment and pan evaporation. Water Resour. Res. 42 (5). https://doi.org/10.1029/2005WR004541. 648-648.

Kendall, M.G., 1975. Rank Correlation Methods. Griffin, London.

Li, X., Wang, L., Chen, D., Yang, K., Wang, A., 2014. Seasonal evapotranspiration changes (1983-2006) of four large basins on the Tibetan Plateau. J. Geophys. Res. 119 (23), 13079–13095. https://doi.org/10.1002/2014JD022380.

Ma, N., Zhang, Y., Szilagyi, J., Guo, Y., Zhai, J., Gao, H., 2015. Evaluating the complementary relationship of evapotranspiration in the alpine steppe of the Tibetan Plateau. Water Resour. Res. 51, 1069–1083. https://doi.org/10.1002/2014WR015493.

Mann, H.B., 1945. Nonparametric tests against trend. Econometrica 13, 245–259. https://doi.org/10.2307/1907187.

McVicar, T.R., VanNiel, T.G., Li, L.T., Hutchinson, M.F., Mu, X.M., Liu, Z.H., 2007. Spatially distributing monthly reference evapotranspiration and pan evaporation considering topographic influences. J. Hydrol. 338, 196–220. https://doi.org/10.1016/j.jhydrol.2007.02.018.

McVicar, T.R., Roderick, M.L., Donohue, R.J., Li, L.T., Niel, T.G.V., Thomas, A., Grieser, J., Jhajharia, D., Himri, Y., Mahowald, N.M., Mescherskaya, A.V., Kruger, A.C., Rehman, S., Dinpashoh, Y., 2012. Global review and synthesis of trends in observed terrestrial near-surface wind speeds: implications for evaporation. J. Hydrol. 416–417 (3), 182–205. https://doi.org/10.1016/j.jhydrol.2011.10.024.

Melillo, J.M., Steudler, P.A., Aber, J.D., Newkirk, A.K., Lux, H., Bowles, F.P., Catricala, C., Magill, A., Ahrens, T., Morrisseau, S., 2002. Soil warming and carbon-cycle feedbacks to the climate system. Science 298, 2173–2176. https://doi.org/10.1126/science.1074153.

Menzel, A., Sparks, T.H., Estrella, N., et al., 2006. European phenological response to climate change matches the warming pattern. Glob. Change Biol. 12, 1969–1976. https://doi.org/10.1111/j.1365-2486.2006.01193.x.

Miller-Rushing, A.J., Hoye, T.T., Inouye, D.W., Post, E., 2010. The effects of phonological mismatches on demography. Philos. Trans. Biol. Sci. 365, 3177–3186.

Monin, A., Obukhov, A., 1954. Basic laws of turbulent mixing in the surface layer of the atmosphere. Contrib. Geophys. Inst. Acad. Sci. USSR 151, 163–187.

Monteith, J.L., 1965. Evaporation and environment. In: Fogg, G.E. (Ed.), State and Movement of Water in Living Organisms, 19th. Symposium Society for Experimental Biology. Cambridge University Press, pp. 205–234.

Morin, X., Viner, D., Chuine, I., 2008. Tree species range shifts at a continental scale: new predictive insights from a process-based model. J. Ecol. 96, 784–794.

Morton, F.I., 1969. Potential evaporation as a manifestation of regional evaporation. Water Resour. Res. 5, 1244–1255. https://doi.org/10.1029/WR005i006p01244.

Niu, S., Wu, M., Han, Y., Xia, J., Li, L., Wan, S., 2008. Water-mediated responses of ecosystem carbon fluxes to climatic change in a temperate steppe. New Phytol. 177, 209–219. https://doi.org/10.1111/j.1469-8137.2007.02237.x.

Peng, S., Piao, S., Ciais, P., Myneni, R.B., Chen, A., Chevallier, F., Dolman, A.J., Janssens, I.A., Peñuelas, J., Zhang, G., Vicca, S., Wan, S., Wang, S., Zeng, H., 2013. Asymmetric effects of daytime and night-time warming on Northern Hemisphere vegetation. Nature 501 (88). https://doi.org/10.1038/nature12434.

Penman, H.L., 1956. Evaporation, an introductory survey. Neth. J. Agr. Sci. 4, 9–29.

Price, J.C., 1991. Timing of NOAA afternoon passes. Int. J. Remote Sens. 12 (1), 193–198.

https://doi.org/10.1080/01431169108929644.
Priestley, C.H.B., Taylor, R.J., 1972. On the assessment of surface heat flux and evaporation using large-scale parameters. Mon. Weather Rev. 100, 81–92.
Rodell, M., Houser, P.R., Jambor, U., Gottschalck, J., Mitchell, K., Meng, C.J., Arse-nault, K., Cosgrove, B., Radakovich, J., Bosilovich, M., Entin, J.K., Walker, J.P., Lohmann, D., Toll, D., 2004. The global land data assimilation system. Bull. Am. Meteorol. Soc. 85 (3), 381–394.
Roderick, M.L., Farquhar, G.D., 2011. A simple framework for relating variations in runoff to variations in climatic conditions and catchment properties. Water Resour. Res. 47https://doi.org/10.1029/2010WR009826. W00G07.
Roderick, M.L., Hobbins, M.T., Farquhar, G.D., 2009. Pan evaporation trends and the terrestrial water balance. Ii. Energy balance and interpretation. Geogr. Compass 2 (3), 761–780.
Sherry, R.A., Weng, E., Arnone, J.A., Johnson, D.W., Schimel, D.S., Verburg, P.S., Wallace, L.L., Luo, Y., 2008. Lagged eff ;ects of experimental warming and doubled precipitation on annual and seasonal aboveground biomass production in a tallgrass prairie. Global Change Biol. 14, 2923–2936.
Staylor, W.F., 1990. Degradation rates of the AVHRR visible channel for the NOAA 6, 7, and 9 spacecraft. J. Atmos. Ocean. Technol. 7, 411–423. https://doi.org/10.1175/1520-0426(1990)007<0411:DROTAV>2.0.CO;2.
Tan, J., 2015. Seasonally different response of photosynthetic activity to daytime and night-time warming in the northern hemisphere. Glob. Change Biol. 21 (1), 377–387. https://doi.org/10.1111/gcb.12724.
Teuling, A.J., Hirschi, M., Ohmura, A., Wild, M., Reichstein, M., Ciais, P., Buchmann, N., Ammann, C., Montagnani, L., Richardson, A.D., Wohlfahrt, G., Seneviratne, S.I., 2009. A regional perspective on trends in continental evaporation. Geophys. Res. Lett. 36https://doi.org/10.1029/2008GL036584. L02404.
Thornthwaite, C.W., 1948. An approach towards a rational classification of climate. Geogr. Rev. 38, 55–94.
Tucker, C.J., Pinzon, J.E., Brown, M.E., Slayback, D.A., Pak, E.W., Mahoney, R., Vermote, E.F., Saleous, N.E., 2005. An extended AVHRR 8-km NDVI dataset compatible with MODIS and SPOT vegetation NDVI data. Int. J. Remote Sens. 26, 4485–4498. https://doi.org/10.1080/01431160500168686.
Turnbull, M.H., Murthy, R., Griffin, K.L., 2002. The relative impacts of day-time and night-time warming on photosynthetic capacity in Populus deltoides. Plant Cell Environ. 25, 1729–1737. https://doi.org/10.1046/j.1365-3040.2002.00947.x.
Vautard, R., Cattiaux, J., Yiou, P., Thépaut, J.N., Ciais, P., 2010. Northern hemisphere atmospheric stilling partly attributed to increased surface roughness. Nat. Geosci. 3 (11), 756–761.
Wang, W., Shao, Q., Peng, S., Xing, W., Yang, T., Luo, Y., Yong, B., Xu, J., 2012. Reference evapotranspiration change and the causes across the Yellow River Basin during 1957-2008 and their spatial and seasonal differences. Water Resour. Res. 48 (5), 113–122. https://doi.org/10.1029/2011WR010724.
Wang, W., Xing, W., Shao, Q., Yu, Z., Peng, S., Yang, T., Yong, B., Taylor, J., Singh, V.P., 2013. Changes in reference evapotranspiration across the Tibetan Plateau: observations and future projections based on statistical downscaling. J. Geophys. Res. Atmos. 118 (10), 4049–4068. https://doi.org/10.1002/jgrd.50393.
Wang, W., Zou, S., Shao, Q., Xing, W., Chen, X., Jiao, X., Luo, Y., Yong, B., Yu, Z., 2016. The analytical derivation of multiple elasticities of runoff to climate change and catchment characteristics alteration. J. Hydrol. 541, 1042–1056. https://doi.org/10.1016/j.jhydrol.2016.08.014.
Xia, J., Chen, J., Piao, S., Ciais, P., Luo, Y., Wan, S., 2014. Terrestrial carbon cycle affected by non-uniform climate warming. Nat. Geosci. 7 (3), 173–180. https://doi.org/10.1038/NGEO2093.
Xie, H., Zhu, X., 2012. Reference evapotranspiration trends and their sensitivity to climatic change on the Tibetan Plateau (1970-2009). Hydrol. Process. 27 (25), 3685–3693. https://doi.org/10.1002/hyp.9487.
Xing, W., Wang, W., Shao, Q., Yong, B., 2018. Identification of dominant interactions between climatic seasonality, catchment characteristics and agricultural activities on Budyko-type equation parameter estimation. J. Hydrol. 556, 585–599. https://doi.org/10.1016/j.jhydrol.2017.11.048.
Xu, C.Y., Gong, L.B., Jiang, T., Chen, D.L., Singh, V.P., 2006. Analysis of spatial distribution and temporal trend of reference evapotranspiration and pan evaporation in Changjiang (Yangtze River) catchment. J. Hydrol. 327, 81–93. https://doi.org/10.1016/j.jhydrol.2005.11.029.
Xu, S., Yu, Z., Ji, X., Sudicky, E.A., 2017. Comparing three models to estimate transpiration of desert shrubs. J. Hydrol. 550, 603–615. https://doi.org/10.1016/j.jhydrol.2017.05.027.
Xu, S., Yu, Z., Zhang, K., Ji, X., Yang, C., Sudicky, E.A., 2018. Simulating canopy conductance of the *Haloxylon ammodendron* shrubland in an arid inland river basin of northwest China. Agric. Forest. Meteorol. 249, 22–34. https://doi.org/10.1016/j.agrformet.2017.11.015.
Xue, B.L., Wang, L., Li, X., Yang, K., Chen, D., Sun, L., 2013. Evaluation of evapotranspiration estimates for two river basins on the Tibetan Plateau by a water balance method. J. Hydrol. 492 (492), 290–297. https://doi.org/10.1016/j.jhydrol.2013.04.005.
Yao, T., Thompson, L., Yang, W., Yu, W., Gao, Y., Guo, X., Yang, X., Duan, K., Zhao, H., Xu, B., Pu, J., Lu, A., Xiang, Y., Kattel, D.B., Joswiak, D., 2012. Different glacier status with atmospheric circulations in Tibetan Plateau and surroundings. Nat. Clim. Change 2 (9), 663–667. https://doi.org/10.1038/nclimate1580.
Ye, J., Guo, A., 2009. Statistical Analysis of Reference Evapotranspiration on the Tibetan Plateau. J. Irrig. Drain. Eng. 135 (2), 134–140. https://doi.org/10.1061/(ASCE)0733-9437(2009)135:2(134).
Zhang, Y., Liu, C., Tang, Y., Yang, Y., 2007. Trends in pan evaporation and reference and actual evapotranspiration across the Tibetan plateau. J. Geophys. Res. Atmos. 112 (D12). https://doi.org/10.1029/2006JD008161.
Zhang, Y., Peña-Arancibia, J.L., McVicar, T., Chiew, F.H.S., Vaze, J., Liu, C., Lu, X., Zheng, H., Wang, Y., Liu, Y.Y., Miralles, D.G., Pan, M., 2016. Multi-decadal trends in global terrestrial evapotranspiration and its components. Sci. Rep. 6https://doi.org/10.1038/srep19124. 19124.